DOI: 10.31276/VJSTE.64(3).38-43

Comparative studies of relaxor-ferroelectric $Pb_{0.92}La_{0.08}(Zr_{0.52}Ti_{0.48})O_3$ thin films deposited by pulsed laser deposition and sol-gel spin coating

Thi Ha Dang[1, 2, 3*], Thi Doan Tran[1], Duc Minh Nguyen[1, 4], Van Truong Do[2], Ngoc Hung Vu[1]

[1]*International Training Institute for Materials Science, Hanoi University of Science and Technology, Vietnam*
[2]*School of Mechanical Engineering, Hanoi University of Science and Technology, Vietnam*
[3]*Vietnam National University of Forestry, Vietnam*
[4]*MESA+ Institute for Nanotechnology, University of Twente, Netherlands*

Received 8 June 2021; accepted 2 August 2021

Abstract:

In this study, the energy storage properties of relaxor $Pb_{0.92}La_{0.08}(Zr_{0.52}Ti_{0.48})O_3$ (PLZT) thin films grown on Pt/Si substrates using pulsed laser deposition (PLD) and sol-gel methods were investigated. The PLZT thin films deposited by PLD possessed a columnar growth microstructure and mixed orientations of (100) and (110) while a dense microstructure and preferred orientation of (100) were achieved by sol-gel deposition. Although the electric breakdown strength (E_{BD}) of the sol-gel-deposited PLZT thin films (E_{BD}=2200 kV/cm) was slightly higher than that of the films deposited using PLD (E_{BD}=2100 kV/cm), the PLD-deposited PLZT thin films had a larger recoverable energy storage density (U_{reco}) and energy storage efficiency (η), which can be explained by its slimmer polarization loop, higher maximum polarization, and lower remanent polarization. At corresponding E_{BD} values, the U_{reco} and η values were 33.2 J/cm^3 and 67.5% for the PLD-deposited films and 27.5 J/cm^3 and 62.2% for the sol-gel-deposited films. Although the sol-gel-deposited PLZT thin films had lower energy storage performance, the sol-gel method remains a promising method for the fabrication of thin films for dielectric energy storage applications due to its unique advantages of low fabrication cost, simple preparation process, and easy control of chemical composition.

Keywords: **energy storage performance, pulsed laser deposition, relaxor ferroelectrics, sol-gel, thin film capacitors.**

Classification number: **2.3**

Introduction

Dielectric capacitors have attracted great attention as pulse-power energy storage devices due to their high power density, fast charge/discharge speed, and excellent thermal and cycling stabilities compared with other energy storage systems such as fuel, chemical batteries, and electromechanical capacitors [1-5]. Indeed, dielectric thin film capacitors with improved performance are becoming eagerly demanded as microelectronics devices are rapidly developing toward miniaturization, light weight, and easy integration. Moreover, dielectric materials in film form usually show an increased electric breakdown strength, which gives rise to larger energy storage density as compared with their bulk-ceramic counterpart [3, 6]. Among dielectric thin film capacitors, relaxor-ferroelectric (RFE) thin films have been extensively investigated due to their slim polarization hysteresis (P-E) loop, low remanent polarization (P_r), low coercive field (E_c), and high breakdown strength (E_{BD}). These properties are a result of a phase transition from a long-range ordered polar state with macroscopic domains in normal ferroelectrics (FEs) to a short-range polar state with nano-scale domains (known as polar nanoregions, or PNRs) in RFEs [7-10], which makes them good candidates for energy storage applications [11-14]. Another feature that distinguishes FEs from RFEs is the frequency dependence of the dielectric constant versus temperature. Dielectric studies on FEs indicate a narrow dielectric constant peak at a high transition temperature (T_m), which corresponds to the maximum value of the dielectric constant. Meanwhile, the existence of a broadened phase transition peak in the temperature-dependent dielectric constant is observed in RFEs [15-17].

*Corresponding author: Email: danghaktck@gmail.com

In general, the volumetric energy storage density (U_{store}), recoverable energy storage density (U_{reco}), and energy storage efficiency (η) of a dielectric capacitor can be calculated from the *P-E* loop as follows [18]:

$$U_{store} = \int_0^{P_{max}} EdP \quad (1)$$

$$U_{reco} = \int_{P_r}^{P_{max}} EdP \quad (2)$$

$$\eta(\%) = 100 \times U_{reco}/U_{store} \quad (3)$$

where P_r and P_{max} are the remanent polarization and maximum polarization (polarization at the maximum applied electrical field E_{max}), respectively.

There are various methods that can be used to fabricate perovskite-oxide ferroelectric thin films such as PLD [19, 20], electron beam deposition [21], sputtering [22], and sol-gel spin coating [23-25]. Among these methods, ferroelectric thin films grown by PLD exhibit excellent ferroelectric and piezoelectric properties [26-29]. However, all methods except sol-gel spin coating require advanced and expensive equipment. Therefore, sol-gel spin coating is particularly suitable for ferroelectric thin film fabrication because of its simplicity, low cost, and, more importantly, easy-to-control stoichiometry and composition in multicomponent films.

In this study, we compared the ferroelectric and energy storage properties of relaxor $Pb_{0.92}La_{0.08}(Zr_{0.52}Ti_{0.48})O_3$ (PLZT) thin films grown on (111)Pt/Ti/SiO_2/Si(100) (Pt/Si) substrates using PLD and sol-gel spin coating. The Pt/Si substrates were chosen because they are widely used in the production of microsystems with ferroelectric films and are well suited to industrial applications [30]. The relaxor behaviour of PLZT films is influenced by the frequency dispersion of the dielectric constant and the increase in T_m with increasing frequency [31]. Experimental results illustrate that E_{BD} slightly improves with a dense microstructure that is accompanied by a degradation of P_{max} and a slight increase of P_r in sol-gel-deposited PLZT thin films. Finally, the U_{reco} and η values achieved in PLZT thin films deposited by PLD were 33.2 J/cm^3 and 67.5% (at E_{BD}=2100 kV/cm), that of the sol-gel method were 27.5 J/cm^3 and 62.2% (at E_{BD}=2200 kV/cm).

Experimental procedure

Fabrication of Pt/Si substrate

For the Pt/Si substrate, a 15-nm-thick Ti adhesive layer and a 100-nm-thick Pt bottom electrode were deposited at room temperature by sputtering on a 500-nm-thick SiO_2 layer formed on a Si(100) substrate using wet oxidation at 1150°C.

Pulsed laser deposition of PLZT thin films

The PLZT thin films were deposited on Pt/Si substrates from a stoichiometric target ($Pb_{0.92}La_{0.08}(Zr_{0.52}Ti_{0.48})O_3$) using PLD. The base pressure of the PLD vacuum chamber was below 10^{-6} mbar. The optimized deposition conditions of the PLZT thin film were a laser repetition rate 10 Hz, energy density 2.5 J/cm^2, oxygen pressure 0.1 mbar, and substrate temperature 600°C [28]. After deposition, the films were cooled to room temperature in a 1-bar oxygen atmosphere with at a ramp rate of 8°C/minute.

Sol-gel spin coating of PLZT thin films

The precursor materials selected for the fabrication of the PLZT thin film by sol-gel consisted of lead acetate trihydrate ($Pb[CH_3COO]_2.3H_2O$), lanthanum nitrate ($La[NO_3]_3$), titanium *iso*-propoxide ($Ti[i\text{-}OPr]_4$), and zirconium *n*-propoxide ($Zr[n\text{-}OPr]_4$). These materials were dissolved in 2-methoxyethanol (MOE) solvent with 15% lead-excess to compensate for lead loss during annealing. The 0.4 M PLZT precursor solution was dripped onto the Pt/Si substrate and spin coated at 2000 rpm for 30 s, followed by pyrolysis at 400°C for 10 min. The number of spin coatings were controlled to achieve a desired thickness, and each coating was about 50 nm thick. Finally, the films were annealed at 650°C for 60 min in air. The final thickness of the films was about 250 nm. More information on sol-gel spin coating of PLZT thin films [32]. The schematic diagram of the PLZT thin film fabricated by the sol-gel method is shown in Fig. 1.

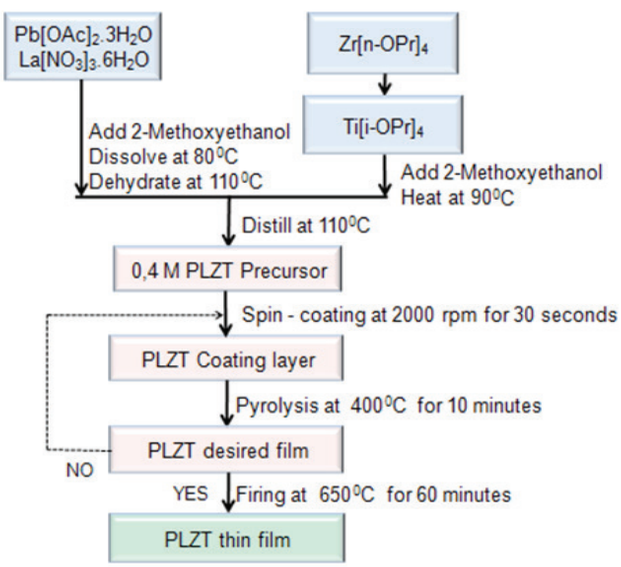

Fig. 1. The schematic representation of the sol-gel spin coating process of PLZT thin films.

Fabrication of thin film capacitors

For electrical measurements, the capacitors (size: 200×200 μm^2) were patterned by a standard photolithography process and structured by argon-beam etching of the Pt top electrodes (100 nm thick), and wet etching of the PLZT films with *HF-HCl* solution to expose the bottom electrodes.

Analysis and characterization

The crystallographic properties of the thin films were analysed by X-ray diffraction (XRD) θ-2θ scans using a PANalytical X-ray diffractometer (Malvern PANalytical) that used Cu-*Kα* radiation with a wavelength of 1.5405 Å. Atomic force microscopy (Bruker Dimension Icon) and cross-sectional high-resolution scanning electron microscopy (HRSEM, Zeiss-1550, Carl Zeiss Microscopy GmbH) were performed to investigate the surface morphology, microstructure, and thickness of the as-grown thin films. The polarization-electric field (*P-E*) hysteresis loops and switching current-electric field (I_{SW}-*E*) curves were collected with using the dynamic hysteresis measurement (DHM) of the ferroelectric module of an aixACCT TF-2000 Analyzer (aixACCT Systems GmbH).

Results and discussion

The XRD pattern shown in Fig. 2A reveals that all the PLZT thin films grown on Pt/Si substrates have the desired perovskite phase without the pyrochlore phase within the detection limit of the XRD. The PLZT thin film deposited by PLD had a (100)/(110) mixed orientation, meanwhile a (100)/(111) mixed orientation was observed in the sol-gel-deposited PLZT thin film. A qualitative analysis of the thin film orientation was calculated as:

$$\%(h00) = 100 \times \frac{(I_{(100)} + I_{200})}{(I_{(100)} + I_{(110)} + I_{(111)} + I_{200})}$$

where *h* (=1, 2) is identical to the one of Miller (*hkl*) indices, and *I* is the intensity of a peak position of the PLZT thin films. The percentages of the (100), (110), and (111) orientations of the sol-gel-deposited PLZT thin film were 63.3, 5.2, and 31.5%, respectively, and 61.5, 38.5, and 0% for the PLZT thin film deposited by PLD. The out-of-plane lattice parameters derived from the corresponding (200) orientation were about 4.027 and 4.042 Å, respectively, for the films deposited using sol-gel and PLD methods. As the out-of-plane lattice parameters in the PLZT thin films were close to the *a*-axis lattice parameters in corresponding PLZT bulk ceramics [33], therefore, it was concluded that the PLZT thin films grown on Pt/Si substrates in this study contained mainly *a*-domains.

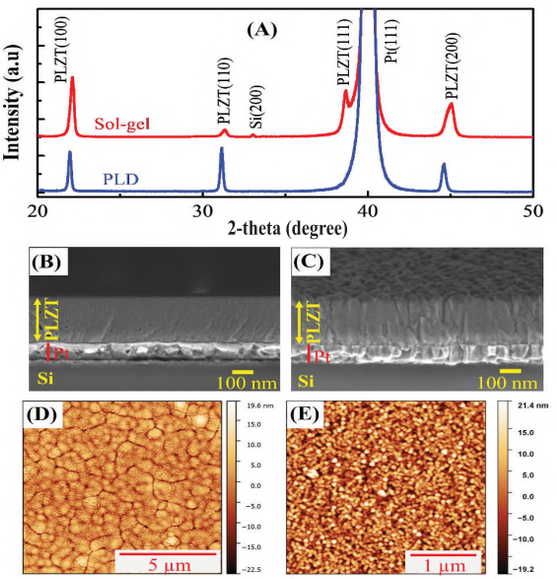

Fig. 2. (A) XRD patterns, (B, C) cross-sectional SEM, and (D, E) surface topographic AFM images of PLZT thin films deposited by sol-gel (B, D) and PLD methods (C, E).

The microstructures of PLZT thin films observed from the cross-sectional SEM and topographic AFM images are shown in Figs. 2B-2E. Figures 2B and 2C indicate that the sol-gel-deposited PLZT thin film had a dense structure while the PLD-deposited film exhibited a columnar structure. The thickness of the PLZT thin films was about 250 nm. The root-mean-square (RMS) surface roughness measured from the AFM images were about 4.4 nm and 7.1 nm for the films deposited by sol-gel and PLD, respectively. The RMS roughness combined with cross-sectional SEM reveal that the films with columnar structure had a larger surface roughness.

Figure 3 shows the *P-E* hysteresis loops and I_{SW}-*E* switching curves of PLZT thin films measured at 1000 kV/cm and 1 kHz. As seen in Fig. 3A, all the *P-E* loops were quite narrow with low P_r and small E_c values. The P_{max}, P_r, and E_c values were 36.04, 6.98 μC/cm^2, and 29.4 kV/cm for the PLZT films deposited by sol-gel and 39.81, 2.06 μC/cm^2, and 42.1 kV/cm for those deposited by PLD. The P_r and E_c values of both films were significantly lower than those of normal ferroelectric $Pb(Zr_{0.52}Ti_{0.48})O_3$ (PZT) thin films, i.e., P_r≈20.65 μC/cm^2 and E_c≈160 kV/cm measured at 1000 kV/cm and 1 kHz, meanwhile, the P_{max} value (≈46.28 μC/cm^2) was slightly higher [32]. In normal FEs, polarization domains have a polarization vector that points along the direction of the applied electric field. The rotation of dipoles is considered to be the main contribution to the total polarization (or P_{max} at the maximum applied field of 1000 kV/cm in this case). When the external electric field is removed, most of the spontaneous polarization will retain the poled direction, which results in a large P_r in normal ferroelectric *P-E*

loops. In contrast, the long-range ordered polar state in RFEs is destroyed, leading to the formation of a short-range polar state with PNRs, which can spontaneously return back to their initial short-range ordered state and result in a small P_r in *P-E* loops [34-36]. These above data confirm the existence of relaxor behaviour in the PLZT thin films in this study.

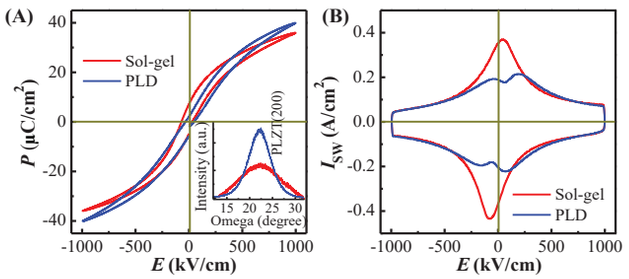

Fig. 3. (A) *P-E* hysteresis loops and (B) I_{sw}-*E* switching current curves of PLZT thin films deposited by sol-gel and PLD methods. Inset in Fig. 3A shows the rocking curves (omega scans) of the PLZT(200) peaks.

Figure 3B presents the corresponding I_{SW}-*E* switching current curves of the PLZT thin films. Another characteristic feature of RFEs is the presence of double-switching peaks corresponding to the coercive field, which was observed in the low electric field region of the sol-gel-deposited PLZT thin films. Meanwhile, in the low electric field region of the I_{SW}-*E* curve of the PLD-deposited thin films, four peaks were observed, which are similar to the I_{SW}-*E* curve of antiferroelectric films but with much higher E_c values [37]. Indeed, the PLD-deposited thin films did exhibit antiferroelectric-like switching behaviour [18]. The difference observed in the I_{SW}-*E* curves of the PLZT thin films in this study can be explained by the change in the crystalline quality of the films. The full width at half maximum (FWHM) of the rocking curve of the PLZT(200) peaks in Fig. 3A inset were 9.7 and 5.5°, respectively, for the PLZT thin films deposited by sol-gel and PLD. The FMHM value is a measure of the range over which the lattice structure in the different grains tilts with respect to the film normal [38] and is therefore an indication of the homogeneity of the films. The crystalline quality of the PLD-deposited PLZT thin films was much better than those deposited by sol-gel. The previous paper indicated that PLZT thin films of better crystalline quality have a larger P_m and lower P_r, as well as a higher intensity of the four switching peaks [20].

In general, the diffuseness factor can be used describe the degree of relaxor behaviour. The diffuseness factor varies from 1 (normal FEs) to 2 (ideal RFEs) [39, 40]. The diffuseness factor in RFEs can be attributed to the film quality in which RFE thin films with higher crystalline quality exhibit a larger diffuseness factor or stronger relaxor behaviour [41].

Similar to Fig. 4 (A, B) shows that both energy storage densities (U_{store} and U_{reco}) and the energy storage efficiency (η) of the PLD-deposited PLZT thin films measured at 1000 kV/cm and 1 kHz are higher than those deposited by sol-gel. This was due to the larger (P_{max}-P_r) value and slimmer *P-E* loop that was just discussed above. Under an applied field of 1000 kV/cm, the U_{reco} and η values were 9.7 J/cm³ and 69.7%, and 13.3 J/cm³ and 74.3%, respectively, for the PLZT thin films deposited by sol-gel and PLD.

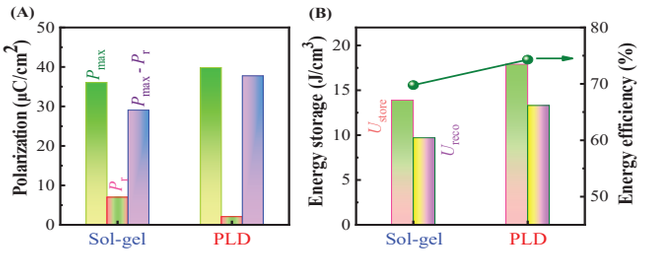

Fig. 4. (A) Polarization (P_{max}, P_r and P_{max}-P_r), (B) energy storage density (U_{store} and U_{reco}), and energy efficiency (η) of PLZT thin films deposited by sol-gel and PLD. The data were derived from the corresponding *P-E* loops in Fig. 3A.

Together with the enhanced recoverable energy storage density and energy storage efficiency, a large electric breakdown strength (E_{BD}) is also necessary to achieve high energy storage density for practical applications. E_{BD} values can be determined from the measurement of a series of capacitors made from each sample by using the Weibull distribution [6, 42-44]:

$$X_i = \ln(E_i) \quad (4)$$

$$Y_i = ln\left(-ln\left[1 - \frac{i}{n+1}\right]\right) \quad (5)$$

where E_i is the breakdown field of capacitor *i* in a series of *n* devices of the same sample type. The breakdown fields are in increasing order, which reflects the decreasing survival chance for a specific field estimated by the value S_i=*(1-i/(n+1))*. The Weibull distribution plots for the breakdown strength of the PLZT thin films are shown in Fig. 5A. Fig. 5B illustrates the thin film capacitors before and after breaking. The critical breakdown strength (taking E_0 as E_{BD}) of a specific type of capacitor is extracted from the intercept of each line with the line Y=0 [12]. As can be seen from Fig. 5A, the E_{BD} values are about 2200 kV/cm and 2100 kV/cm for the PLZT thin films deposited by sol-gel and PLD, respectively. Compared with the PLD-deposited PLZT thin films with a columnar structure, the dense structure leads to a slight increase in breakdown strength in the sol-gel-deposited PLZT thin films.

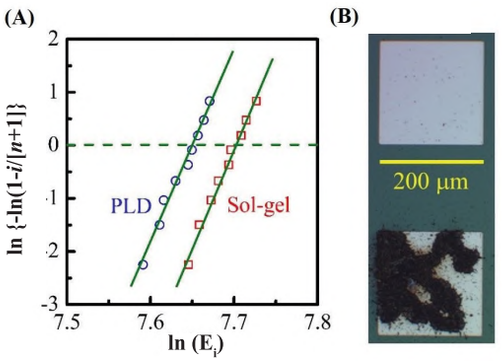

Fig. 5. (A) Weibull distribution of breakdown strength for the capacitors of PLZT thin films deposited by sol-gel and PLD and (B) optical images of thin film capacitors before (upper) and after breaking (lower).

Figure 6 compares the *P-E* hysteresis loops of the PLZT thin films measured at 1000 kV/cm and their corresponding E_{BD} values. Similar to the *P-E* loops measured at 1000 kV/cm, the *P-E* loop of PLD-deposited PLZT thin films at E_{BD} (2100 kV/cm) were slimmer than those deposited by sol-gel (E_{BD}=2200 kV/cm). Moreover, the P_{max} of the *P-E* loop measured at the E_{BD} of the PLD-deposited PLZT thin films was higher than that of the sol-gel PLZT thin films, even as a lower E_{BD} value was achieved in the PLD-deposited films. As a result, the U_{reco} and η values, measured at their corresponding E_{BD}, were 27.5 J/cm^3 and 62.2% for the PLZT thin films deposited by sol-gel and 33.2 J/cm^3 and 67.5% for those deposited by PLD.

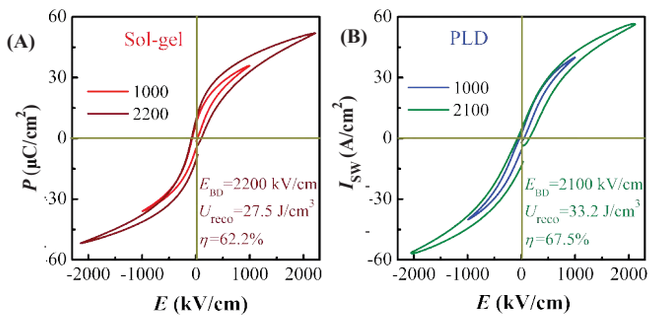

Fig. 6. *P-E* loops of the PLZT thin films deposited by (A) sol-gel and (B) PLD measured at 1000 kV/cm and their corresponding E_{BD} values.

Conclusions

In summary, we studied the ferroelectric properties and energy storage performance of relaxor PLZT thin films deposited on Pt/Si substrates by PLD and sol-gel spin coating. The sol-gel-deposited PLZT thin films with dense structure exhibited a mixed orientation of (100) and (111), meanwhile a mixed orientation of (100) and (110) was observed in the columnar PLZT thin films deposited by PLD. We found that the relaxor behaviour was enhanced with improvements in the crystalline quality of the film. On the other hand, the PLD-deposited PLZT thin films had stronger relaxor behaviour with a slimmer *P-E* loop and lower P_r value due to its higher crystalline quality. Together with a larger P_m, higher U_{reco} and η values were achieved in the PLD-deposited PLZT thin films. Despite the even lower values of U_{reco} (-17%) and η (-8%) obtained in the sol-gel-deposited PLZT thin films, sol-gel can be still an effective method for the development of thin film capacitors for energy storage applications because of their low cost, great versatility in composition, simplicity, and scalable fabrication technique.

ACKNOWLEDGEMENTS

The authors would like to acknowledge the financial support from the National Foundation for Science and Technology Development of Vietnam under grant No. 103.99-2018.23.

COMPETING INTERESTS

The authors declare that there is no conflict of interest regarding the publication of this article.

REFERENCES

[1] K. Han, N. Luo, S. Mao, F. Zhuo, X. Chen, L. Liu, C. Hu, H. Zhou, X. Wang, Y. Wei (2019), "Realizing high low-electric-field energy storage performance in $AgNbO_3$ ceramics by introducing relaxor behaviour", *Journal of Materiomics*, **5**(**4**), pp.597-605.

[2] K. Yao, S. Chen, M. Rahimabady, M.S. Mirshekarloo, S. Yu, F.E.H. Tay, T. Sritharan, L. Lu (2011), "Nonlinear dielectric thin films for high-power electric storage with energy density comparable with electrochemical supercapacitors", *IEEE Transactions on Ultrasonics, Ferroelectrics, Frequency Control*, **58**(**9**), pp.1968-1974.

[3] H. Palneedi, M. Peddigari, G.T. Hwang, D.Y. Jeong, J. Ryu (2018), "High-performance dielectric ceramic films for energy storage capacitors: progress and outlook", *Advanced Functional Materials*, **28**(**42**), DOI: 10.1002/adfm.201803665.

[4] X. Hao (2013), "A review on the dielectric materials for high energy storage application", *Journal of Advanced Dielectrics*, **3**(**1**), DOI: 10.1142/S2010135X13300016.

[5] F. Li, J. Zhai, B. Shen, H. Zeng (2018), "Recent progress of eco-friendly perovskite-type dielectric ceramics for energy storage applications", *Journal of Advanced Dielectrics*, **8**(**6**), DOI: 10.1142/S2010135X18300050.

[6] M.D. Nguyen, E.P. Houwman, M.T. Do, G. Rijnders (2020a), "Relaxor-ferroelectric thin film heterostructure with large imprint for high energy storage performance at low operating voltage", *Energy Storage Materials*, **25**, pp.193-201.

[7] V.V. Shvartsman, D.C. Lupascu (2012), "Lead-free relaxor ferroelectrics", *Journal of the American Ceramic Society*, **95**(**1**), pp.1-26.

[8] L.E. Cross (1994), "Relaxorferroelectrics: An overview", *Ferroelectrics*, **151**(**1**), pp.305-320.

[9] V. Shvartsman, W. Kleemann, J. Dec, Z. Xu, S. Lu (2006), "Diffuse phase transition in $BaTi_{1-x}Sn_xO_3$ ceramics: An intermediate state between ferroelectric and relaxor behaviour", *Journal of Applied Physics*, **99**(**12**), DOI:10.1063/1.2207828.

[10] M.D. Nguyen, G. Rijnders (2020b), "Comparative study of piezoelectric response and energy storage performance in normal ferroelectric, antiferroelectric and relaxor-ferroelectric thin films", *Thin Solid Films*, **697**, DOI: 10.1016/j.tsf.2020.137843

[11] A. Kursumovic, W. W. Li, S. Cho, P. Curran, D. Tjhe, J. MacManus-Driscoll (2020), "Lead-free relaxor thin films with huge energy density and low loss for high temperature applications", *Nano Energy*, **71**, DOI:10.1016/j.nanoen.2020.104536.

[12] M.D. Nguyen (2021), "Ultrahigh energy storage performance in lead-free BZT thin films by tuning relaxor behaviour", *Materials Research Bulletin*, **133**, DOI: 10.1016/j.materresbull.2020.111072.

[13] S. Ji, Q. Li, D. Wang, J. Zhu, M. Zeng, Z. Hou, Z. Fan, X. Gao, X. Lu, Q. Li (2021), "Enhanced energy storage performance and thermal stability in relaxor ferroelectric (1-x)$BiFeO_3$-x(0.85$BaTiO_3$-0.15$Bi(Sn_{0.5}Zn_{0.5})O_3$) ceramics", *Journal of the American Ceramic Society*, **104**(**6**), DOI: 10.1111/jace.17705.

[14] Z. Hu, B. Ma, S. Liu, M. Narayanan, U. Balachandran (2014), "Relaxor behaviour and energy storage performance of ferroelectric PLZT thin films with different Zr/Ti ratios", *Ceramics International*, **40**(**1**), pp.557-562.

[15] A. Kumar, K.J. Raju, A. James (2017), "Diffuse phase transition in mechanically activated $(Pb_{1-x}La_x)(Zr_{0.60}Ti_{0.40})O_3$ electro-ceramics", *Journal of Materials Science: Materials in Electronics*, **28**(**18**), pp.13928-13936.

[16] A. Pramanick, S. Nayak (2021), "Perspective on emerging views on microscopic origin of relaxor behaviour", *Journal of Materials Research*, DOI: 10.1557/s43578-020-00010-7.

[17] V. Shvartsman, J. Dec, Z. Xu, J. Banys, P. Keburis, W. Kleemann (2008), "Crossover from ferroelectric to relaxor behaviour in $BaTi_{1-x}Sn_xO_3$ solid solutions", *Phase Transitions*, **81**(**11-12**), pp.1013-1021.

[18] M.D. Nguyen, E.P. Houwman, G. Rijnders (2018a), "Energy storage performance and electric breakdown field of thin relaxor ferroelectric PLZT films using microstructure and growth orientation control", *The Journal of Physical Chemistry C*, **122**(**27**), pp.15171-15179.

[19] M.D. Nguyen, E.P. Houwman, M. Dekkers, C.T. Nguyen, H.N. Vu, G. Rijnders (2016), "Enhanced energy storage density and energy efficiency of epitaxial $Pb_{0.9}La_{0.1}(Zr_{0.52}Ti_{0.48})O_3$ relaxor-ferroelectric thin films deposited on silicon by pulsed laser deposition", *APL Materials*, **4**(**8**), DOI: 10.1063/1.4961636.

[20] M.D. Nguyen, C.T. Nguyen, H.N. Vu, G. Rijnders (2018b), "Controlling microstructure and film growth of relaxor-ferroelectric thin films for high break-down strength and energy storage performance", *Journal of the European Ceramic Society*, **38**(**1**), pp.95-103.

[21] B. Panda, S. Ray, A. Dhar, A. Sarkar, D. Bhattacharya, K. Chopra (1996), "Electron beam deposited lead-lanthanum-zirconate-titanate thin films for silicon-based device applications", *Journal of Applied Physics*, **79**(**2**), pp.1008-1012.

[22] H. Adachi, K. Wasa (1991), "Sputtering preparation of ferroelectric PLZT thin films and their optical applications", *IEEE Transactions on Ultrasonics, Ferroelectrics, and Frequency Control*, **38**(**6**), pp.645-655.

[23] X. Hao, Y. Wang, J. Yang, S. An, J. Xu (2012), "High energy storage performance in $Pb_{0.91}La_{0.09}(Ti_{0.65}Zr_{0.35})O_3$ relaxor ferroelectric thin films", *Journal of Applied Physics*, **112**(**11**), DOI:10.1063/1.4768461.

[24] L. Zhang, X. Hao, J. Yang, S. An, B. Song (2013), "Large enhancement of energy storage properties of compositional graded $(Pb_{1-x}La_x)(Zr_{0.65}Ti_{0.35})O_3$ relaxor ferroelectric thick films", *Applied Physics Letters*, **103**(**11**), DOI:10.1063/1.4821209.

[25] S. Tong, B. Ma, M. Narayanan, S. Liu, R. Koritala, U. Balachandran, D. Shi (2013), "Lead lanthanum zirconate titanate ceramic thin films for energy storage", *ACS Applied Materials & Interfaces*, **5**(**4**), pp.1474-1480, DOI: 10.1021/am302985u.

[26] M. Dinescu (2010), "PLD of piezoelectric and ferroelectric materials", *Laser - Surface Interactions for New Materials Production*, Springer, pp.307-330.

[27] K.K. Sahoo, R. Katoch, K. Brajesh, A. Garg, R. Gupta (2020), "Improved ferroelectric response of pulsed laser deposited $BiFeO_3$-$PbTiO_3$ thin films around morphotropic phase boundary with interfacial $PbTiO_3$ buffer layer", *Journal of Applied Physics*, **127**(**6**), DOI:10.1063/1.5110335.

[28] M.D. Nguyen, E. Houwman, M. Dekkers, H.N. Vu, G. Rijnders (2014), "A fast room-temperature poling process of piezoelectric $Pb(Zr_{0.45}Ti_{0.55})O_3$ thin films", *Science of Advanced Materials*, **6**(**2**), pp.243-251.

[29] C.T.Q. Nguyen, M.D. Nguyen, M. Dekkers, E. Houwman, H.N. Vu, G. Rijnders (2014), "Process dependence of the piezoelectric response of membrane actuators based on $Pb(Zr_{0.45}Ti_{0.55})O_3$ thin films", *Thin Solid Films*, **556**, pp.509-514.

[30] M.D. Nguyen (2021), "Tuning of microstructure and piezoelectric response of laser ablated $Pb(Zr,Ti)O_3$ films by varying the oxygen deposition pressure", *Ferroelectrics*, **573**(**1**), pp.42-51.

[31] B. Ma, Z. Hu, S. Liu, S. Tong, M. Narayanan, R.E. Koritala, U. Balachandran (2013), "Temperature-dependent dielectric nonlinearity of relaxor ferroelectric $Pb_{0.92}La_{0.08}Zr_{0.52}Ti_{0.48}O_3$ thin films", *Applied Physics Letters*, **102**(**20**), DOI:10.1063/1.4807665.

[32] H.T. Dang, T.T. Trinh, C.T. Nguyen, T.V. Do, M.D. Nguyen, H.N. Vu (2019), "Enhancement of relaxor behaviour by La doping and its influence on the energy storage performance and electric breakdown strength of ferroelectric $Pb(Zr_{0.52}Ti_{0.48})O_3$ thin films", *Materials Chemistry Physics*, **234**, pp.210-216.

[33] P.S. Janrao, V. Mathe (2017), "Phase tuning in lanthanum doped lead zirconate titanate near morphotropic phase boundary using chemical co-precipitation route and their dielectric properties", *Journal of Materials Science: Materials in Electronics*, **28**(**1**), pp.1078-1085.

[34] Q. Hu, X. Wei (2019), "Abnormal phase transition and polarization mismatch phenomena in $BaTiO_3$-based relaxor ferroelectrics", *Journal of Advanced Dielectrics*, **9**(**5**), DOI: 10.1142/S2010135X19300020.

[35] L. Yang, J. Xu, Q. Li, W. Zeng, C. Zhou, C. Yuan, G. Chen, G. Rao (2016), "High piezoelectricity associated with crossover from nonergodicity to ergodicity in modified $Bi_{0.5}Na_{0.5}TiO_3$ relaxor ferroelectrics", *Journal of Electroceramics*, **37**(**1**), pp.23-28.

[36] Z. Yang, H. Du, L. Jin, Q. Hu, H. Wang, Y. Li, J. Wang, F. Gao, S. Qu (2019), "Realizing high comprehensive energy storage performance in lead-free bulk ceramics via designing an unmatched temperature range", *Journal of Materials Chemistry*, **7**(**48**), pp.27256-27266.

[37] M.D. Nguyen, G. Rijnders (2018c), "Electric field-induced phase transition and energy storage performance of highly-textured $PbZrO_3$ antiferroelectric films with a deposition temperature dependence", *Journal of the European Ceramic Society*, **38**(**15**), pp.4953-4961.

[38] H. Funakubo, M. Dekkers, A. Sambri, S. Gariglio, I. Shklyarevskiy, G. Rijnders (2012), "Epitaxial PZT films for MEMS printing applications", *APL Materials*, **37**(**11**), pp.1030-1038.

[39] Z. Shen, X. Wang, B. Luo, L. Li (2015), "$BaTiO_3$-$BiYbO_3$ perovskite materials for energy storage applications", *Journal of Materials Chemistry A*, **3**(**35**), pp.18146-18153.

[40] C. Yang, Y. Han, C. Feng, X. Lin, S. Huang, X. Cheng, Z. Cheng, interfaces (2020), "Toward multifunctional electronics: Flexible NBT-based film with a large electrocaloric effect and high energy storage property", *ACS Applied Materials & Interfaces*, **12**(**5**), pp.6082-6089.

[41] J. Ouyang (2019), *Nanostructures in Ferroelectric Films for Energy Applications*, Elsevier, 386pp.

[42] H. Pan, J. Ma, J. Ma, Q. Zhang, X. Liu, B. Guan, L. Gu, X. Zhang, Y.J. Zhang, L. Li, Y. Shen, Y.H. Lin, C.W. Nan (2018), "Giant energy density and high efficiency achieved in bismuth ferrite-based film capacitors via domain engineering", *Nature Communications*, **9**(**1**), pp.1-8.

[43] Y. Wang, J. Cui, L. Wang, Q. Yuan, Y. Niu, J. Chen, Q. Wang, H. Wang (2017), "Compositional tailoring effect on electric field distribution for significantly enhanced breakdown strength and restrained conductive loss in sandwich-structured ceramic/polymer nanocomposites", *Journal of Materials Chemistry*, **5**(**9**), pp.4710-4718.

[44] Q. Yuan, G. Li, F.Z. Yao, S.D. Cheng, Y. Wang, R. Ma, S.B. Mi, M. Gu, K. Wang, J.F. Li (2018), "Simultaneously achieved temperature-insensitive high energy density and efficiency in domain engineered $BaTiO_3$-$Bi(Mg_{0.5}Zr_{0.5})O_3$ lead-free relaxor ferroelectrics", *Nano Energy*, **52**, pp.203-210.